Short-Term Reliability Assessment of Integrated Power-Gas Systems With Hydrogen Injections Using Universal Generating Function

Sheng Wang, *Member, IEEE,* Hongxun Hui, *Member, IEEE,* Junyi Zhai, *Member, IEEE*

Abstract—**Injecting alternative gas (e.g., green hydrogen from wind generation) into the gas system is a promising way to decarbonize the energy sector. However, the fluctuating renewable generation could lead to time-varying alternative gas injections. Then, the gas composition in the gas system may become uncertain, increasing the short-term risk of the integrated power-gas systems during the operation. This paper proposes a short-term reliability assessment approach for IPGS with alternative gas injections. First, the multi-performance and multi-state universal generating functions (UGF) are constructed to efficiently model the short-term reliability of the power-to-gas facility and the wind farm, respectively. Then, a reliability management UGF operator is proposed to minimize both load shedding and gas security violation. A set of novel reliability indices is proposed to comprehensively assess the gas security violations under uncertain gas compositions. Moreover, an analytical short-term reliability assessment approach is proposed, where the state-based sequential approximation and state-based McCormick envelope techniques are tailored and embedded. By optimizing the solution order by the system states, the nonconvexities in the reliability management optimization problem can be handled tractably without increasing the computation burden. Finally, the IEEE 24 bus Reliability Test System and the Belgium gas system are used to validate the proposed approach.**

Index Terms—**integrated power and gas systems, gas composition, hydrogen, short-term reliability, renewable energy, power-to-gas**

I. INTRODUCTION

ALTERNATIVE gas (including green hydrogen, methane, etc.) can be produced sustainably by consuming renewable generations via power-to-gas (PTG) facilities. The large-scale use of alternative gas is regarded as a promising way to deliver net-zero ambition in many countries [1]. For example, China has published mid and long-term planning for the development hydrogen industry, which aims to achieve 100-200 kiloton renewable hydrogen production, and reduce carbon dioxide emission by 1-2 million tons per year by 2025

[2]. The production of green alternative gas can also be used to accommodate surplus renewable energies. Therefore, to promote the overall benefits during alternative gas production, the power and gas systems need to be operated coordinately, and the concept of integrated power-gas systems (IPGS) has been developed.

Using the existing natural gas pipelines is one of the most cost-benefit ways to transport the alternative gas produced by PTGs. Besides the lower cost, it shows a lot of other benefits, such as decarbonizing the gas system, increasing the robustness of the gas system by charging the linepacks, etc [3]. However, it also has negative impacts and increases the operational risk of the IPGS. On the one hand, the fluctuating wind generation will lead to the fluctuating injection of hydrogen into the gas system. The gas composition across the gas network may become time-varying and uncertain. However, gas appliances (e.g., gas water heaters), which use gas for combustion to produce heat energy, usually require a steady gas composition. The change in the gas composition may lead to unideal combustion, flashbacks, etc [4]. On the other hand, the varying gas composition will change the physical properties (e.g., specific gravity, etc.) of the gas mixtures in the gas network. It may cause additional damage, affecting the lifespan of IPGS components (e.g., pipeline valves) [5]. It may also change the gas flow patterns, and cause oscillations in the gas network [6]. Therefore, the impacts of alternative gas injections on the short-term reliability of IPGS need to be contained and evaluated from a holistic perspective of view.

The impacts of alternative gas through PTGs have been analyzed in some previous studies. The impacts of PTGs on the operation of IPGS are investigated in [7]. The flexibility of the integrated electricity-gas-hydrogen system with PTG is explored in [8]. The probabilistic multi-energy flow model of electricity and gas is developed considering hydrogen injection in [9]. The influence of different hydrogen blending modes on the IPGS is simulated in [10]. The simulation is further extended into transient state analysis to investigate the propagation of hydrogen content in the pipeline in [11]. However, in these studies, either the impacts of hydrogen injections from PTGs on the gas composition in the gas network are not considered, or the system operator just acts as a receiver of alternative gas. They do not take active measures to mitigate the negative impacts of alternative gas, which makes these evaluations less practical.

Recently, there are several studies begin to focus on regulating the gas composition from an optimal energy flow perspective. The distributional robust operation model of IPGS with hydrogen injections is proposed in [12] considering wind fluctuations. The model is also applied to the volt-var-pressure

optimization in [13]. The integrated optimization model with gas composition tracking in the IPGS with hydrogen injections is developed in [14]. The detailed security-constrained optimal energy flow model in IPGS with alternative gas injections is proposed in [15]. However, these studies focus on regulating the gas composition in deterministic scenarios, while the short-term reliability under various uncertainties cannot be assessed comprehensively.

Concluding the above research, there are still some challenges that remain unaddressed for the reliability assessment of IPGS with alternative gas. First, the off-the-shelf reliability model of PTG used in the traditional IPGS with constant gas composition is relatively rough, which cannot be applied directly to the IPGS with alternative gas injections [16]. By considering different alternative gas production modes, the PTG can be modeled as a multi-performance system. The multiple performance degradation of PTG with different subsystem failures has not been investigated yet [17]. Second, the impacts of varying gas compositions on the physical model of the IPGS have not been thoroughly investigated. References [12], [13] conduct the optimal energy flow with alternative gas injections, but the impacts of varying gas composition on the physical properties of gas mixtures are neglected. The reliability of IPGS is evaluated in [18], but the hydrogen injections are also pre-specified, which is not in line with the real system. Third, there lack of indices that can characterize the short-term reliability of IPGS with alternative gas injections. The traditional gas security indices, such as the Wobbe index, flame speed factors, etc., are usually used to characterize the gas interchangeability under a given condition with alternative gas injections [19]. However, these indices can not be directly applied to the assessment of IPGS reliabilities under stochastic conditions [20].

To address the research gaps, this paper firstly proposes a short-term reliability assessment approach for IPGS to evaluate the impacts of alternative gas injections. The contributions are summarised as follows [21]:

1) An short-term reliability model of PTG is proposed by using the UGF method. The UGFs of the detailed gas production processes, including the electrolysis, methanation, purifications, etc., of methane and hydrogen are formulated. Compared with the traditional enumeration method, the proposed method can model the time-varying multi-performance of the PTG system in an efficient and unified way.
2) A reliability management UGF operator is proposed, which can mitigate both load shedding and gas composition deviations. The power and gas systems are coordinated to improve both the operating mode of PTGs and the accommodation of renewable energy. Compared with traditional impact analysis of alternative gas injections, this paper models the gas composition as variables, so that the time-varying physical properties of gas mixtures can be better revealed.
3) Novel short-term reliability indices are proposed. By extending the traditional deterministic gas security indices, such as the Wobbe index, flame speed factor, etc., the proposed short-term reliability indices can better
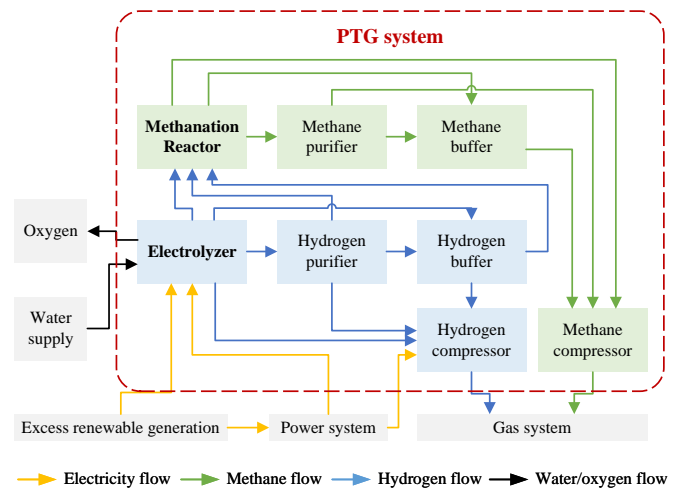

Fig. 1. Structure of the PTG system.

TABLE I
FUNCTIONS OF PTG'S SUBSYSTEMS

Subsystem	Function
Electrolyzer	Consume electricity to produce hydrogen
Hydrogen purifier	Remove impurities(e.g., water vapor) in hydrogen production
Hydrogen buffer	Temporarily store hydrogen production
Hydrogen compressor	Increase the pressure of hydrogen
Methanation reactor	Consume electricity to produce hydrogen
Methane purifier	Remove impurities(e.g., hydrogen) in methane production
Methane buffer	Temporarily store methane production
Methane compressor	Increase the pressure of methane

measure the expectations of gas securities under various uncertainties.
4) A tractable short-term reliability assessment method is developed. By proposing state-based sequential approximation and McCormick envelope techniques, the nonlinearities in the reliability management optimization problem (Weymouth equation, gas mixing equation, etc.) can be convexified without increasing the computation burden.

II. SHORT-TERM RELIABILITY MODELS OF COMPONENTS

A. Multi-performance short-term reliability model of PTG

The structure of the PTG system is presented in Fig. 1. It contains eight subsystems, including the methane reactor, electrolyzer, methane and hydrogen purifiers, buffers, and compressors. Their functions are presented in Table. I. The PTG is supplied with water and electricity to produce hydrogen via the electrolysis process. Then, the produced hydrogen will go through the purifier and buffer. Then, the hydrogen will be compressed and injected into the gas system, or go through the methanation process. The produced methane will also be purified, compressed, and injected into the gas network.

The reliability of the PTG system relies on the reliability of the subsystems. The short-term reliabilities of these subsystems can be represented by binary state models. Each of them has two states, namely, the normal state and the failure state. Take the electrolyzer as an example, its UGF can be written as [22]:

$$u_{i,l}^{el}(z) = A_{i,l}^{el}(t)z^{s^{el}} + U_{i,l}^{el}(t)z^{1-s^{el}} \tag{1}$$

TABLE II
CONSEQUENCE OF FAILURE FOR DIFFERENT PTG SUBSYSTEMS

Performance indicator	Failure of subsystem							
	Electrolyzer	Hydrogen purifier	Hydrogen buffer	Hydrogen compressor	Methanation reactor	Methane purifier	Methane buffer	Methane compressor
Hydrogen production capacity	×	✓	✓	×	✓	✓	✓	✓
Hydrogen purity	×	×	✓	×	✓	✓	✓	✓
Hydrogen storage capacity	×	✓	×	×	✓	✓	✓	✓
Methane production capacity	×	✓	✓	✓	×	✓	✓	×
Methane purity	×	×	✓	✓	×	×	✓	×
Methane storage capacity	×	✓	✓	✓	×	✓	×	×

✓ indicates that the performance is still at the normal state with the failure of the subsystem;
× indicates that the performance is at the failure state with the failure of the subsystem.

where $u_{i,l}^{el}(z)$ is the UGF of electrolyzer of PTG l at bus i; z represents the z-transformation [23]; $A_{i,l}^{el}$ and $U_{i,l}^{el}$ are the availability and unavailability of the electrolyzer, respectively; s^{el} is the state indicator for electrolyzer, where $s^{el} = 1$ and 0 represent the normal state and failure state, respectively.

The transition between the two states is modeled by a time-continuous Markov process. Therefore, during the operation, the availability and unavailability are functions of time:

$$A_{i,l}^{el}(t) = \frac{\mu_{i,l}^{el}}{\mu_{i,l}^{el} + \lambda_{i,l}^{el}} + \frac{\lambda_{i,l}^{el}}{\mu_{i,l}^{el} + \lambda_{i,l}^{el}} e^{-(\mu_{i,l}^{el} + \lambda_{i,l}^{el})t} \quad (2)$$

$$U_{i,l}^{el}(t) = \frac{\lambda_{i,l}^{el}}{\mu_{i,l}^{el} + \lambda_{i,l}^{el}} \left(1 - e^{-(\mu_{i,l}^{el} + \lambda_{i,l}^{el})t}\right) \quad (3)$$

where $\lambda_{i,l}^{el}$ and $\mu_{i,l}^{el}$ are the failure and repair rates of the electrolyzer of PTG l at bus i, respectively.

The failure of different subsystems can lead to different kinds of degradation for the PTG system. There are six indicators to measure the performance of a PTG system, i.e., hydrogen production capability, purity, and storage capacity, as well as methane production capability, purity, and storage capacity. They are denoted as performance h, $h = 1, ..., 6$, respectively. Each performance has two states, i.e., the normal state and the failure state. Therefore, the PTG system can be represented as a multi-performance binary-state reliability model. The relationships between subsystem failure and performance degradation can be seen in Table. II.

The state indicator of each performance can be represented by the structure function of the states of the subsystems. For example, the state indicator of the hydrogen production capacity can be written as:

$$s_1 = s^{el} s^{hc} \quad (4)$$

where s_1, s^{el}, and s^{hc} are the state indicators for hydrogen production capacity, electrolyzer, and hydrogen compressor, respectively.

According to the structure function, the UGF of hydrogen production capacity performance can be formed as [24]:

$$
\begin{aligned}
u_{i,l}^1(z) =& \Omega^s \left\{ u_{i,l}^{el}(z), u_{i,l}^{hc}(z) \right\} \\
=& \Omega^s \left\{ A_{i,l}^{el} z^{s^{el}} + U_{i,l}^{el} z^{1-s^{el}}, A_{i,l}^{hc} z^{s^{hc}} + U_{i,l}^{hc} z^{1-s^{hc}} \right\} \\
=& A_{i,l}^{el} A_{i,l}^{hc} z^{s^{el} s^{hc}} + A_{i,l}^{el} U_{i,l}^{hc} z^{s^{el}(1-s^{hc})} \\
&+ U_{i,l}^{el} A_{i,l}^{hc} z^{(1-s^{el})s^{hc}} + U_{i,l}^{el} U_{i,l}^{hc} z^{(1-s^{el})(1-s^{hc})} \quad (5)
\end{aligned}
$$

where $u_{i,l}^1(z)$ is the UGF of hydrogen production capacity for PTG l at bus i; $u_{i,l}^{hc}(z)$ is the UGF of hydrogen compressor; Ω^s is the series operator; $A_{i,l}^{hc}$ and $U_{i,l}^{hc}$ are the availability and unavailability of hydrogen compressor, respectively, which are functions of time.

Based on this UGF, the availability, and unavailability of the hydrogen production capacity, $A_{i,l}^1$ and $U_{i,l}^1$, can be calculated as:

$$A_{i,l}^1 = \left. \frac{\partial u_{i,l}^1(z)}{\partial z} \right|_{s_1=1, z=1}, \ U_{i,l}^1 = \left. \frac{\partial u_{i,l}^1(z)}{\partial z} \right|_{s_1=0, z=1} \quad (6)$$

The state probabilities of other performances can be derived similarly. After obtaining the state probabilities of all performances, the multi-performance UGF of the PTG system can be derived:

$$u_{i.l}^{ptg}(z) = \sum_{h \in \mathcal{H}} A_{i,l}^{ptg,h} z_h^{s_h} + U_{i,l}^{ptg,h} z_h^{1-s_h} \quad (7)$$

where $u_{i.l}^{ptg}(z)$ is the UGF function of PTG l at bus i; z_h represents z-transformation of performance h; $\mathcal{H}$ is the set of performances; $A_{i,l}^{ptg,h}$ and $U_{i,l}^{ptg,h}$ are the availability and unavailability of the performance h of the PTG, respectively; s_h is the state indicator for performance h. Then, the state probability of performance h can be calculated as $\partial u_{i,l}^{ptg}(z_h)/\partial z_h$.

The feasible region of PTG varies with the degradations of different performances. Thus, we have [25]:

$$\boldsymbol{q}_{i,l}^{ptg} \in \boldsymbol{\mathcal{Q}}_{i,l}(\boldsymbol{s}) \quad (8)$$

where $\boldsymbol{q}_{i,l}^{ptg}$ represents the operating condition of PTG l at bus i; $\boldsymbol{\mathcal{Q}}(\boldsymbol{s})_{i,l}$ is the feasible region for PTG operation, where $\boldsymbol{s} = \{s_1, ..., s_6\}$. The detailed model can be found in Appendix.A.

B. Multi-state short-term reliability model of wind farm

The wind speed during the operation is a series $v_i = \{v_{i,1}, ..., v_{i,k}, ..., v_{i,K}\}$, where K is the number of time steps. Its value at a specific time point k can be modeled as the combination of the forecast value and the deviation:

$$v_{i,k} = \overline{v}_{i,k} + \Delta v_{i,k} \quad (9)$$

where $\overline{v}_{i,k}$ is the center value of the wind speed at time step k at bus i; $\Delta v_{i,k}$ is the deviation to the center value.

While the center value can be derived by the summed average of historical wind speed, the deviation part is varying with time. Therefore, we model the stochastic process of wind speed deviations as a Markov process. According to the

historical data, the wind speed deviations can be clustered into S states $\Delta v_i^s, s \in \mathcal{S}$. The state probabilities can be calculated by solving the following partial derivative equations [26]:

$$
\begin{cases}
\dfrac{d\mathrm{Pr}_i^{wd,s}(t)}{dt} = -\mathrm{Pr}_i^{wd,s}(t)\sum_{s'=1}^{S,s'\neq s}\lambda_{s,s'}^{wd} \\
\qquad + \sum_{s'=1}^{S,s'\neq s}\mathrm{Pr}_i^{wd,s'}(t)\lambda_{s',s}^{wd}, s=1,2,...,S \\
\mathrm{Pr}_i^1|_{t=0}=0,...,\mathrm{Pr}_i^{s_0}|_{t=0}=1,...,\mathrm{Pr}_i^S|_{t=0}=0
\end{cases}
\tag{10}
$$

where $\mathrm{Pr}_i^{wd,s}(t)$ is the probability of wind speed being in state s; $\lambda_{s,s'}^{wd}$ is the state transition rate of wind from state s to state s'; s_0 is the initial state of wind.

The power generation of the wind farm is not only associated with the wind speed, but also with the internal states of the wind turbines. Generally, a wind farm at bus i has L_i^{wt} wind turbines. The reliability of each wind turbine is represented by a binary state model. Thus, the reliability of the wind farm can be represented by a multi-state model. The structure function can be written as [27]:

$$
s^{wf} = \sum_{l\in\mathcal{L}_i^{wt}} s^{wd} s_l^{wt}
\tag{11}
$$

where s^{wf} and s_l^{wt} are the state indicators of the wind farm and wind turbine l, respectively.

The UGF of the wind turbine $u_{i,l}^{wt}(z)$ can be written as [26]:

$$
\begin{aligned}
u_{i,l}^{wt}(z) &= \Omega^s\left\{u_{i,l}^{wi}(z), u_i^{wd}(z)\right\} \\
&= \Omega^s\left\{A_{i,l}^{wt}z^{s^{wt}} + U_{i,l}^{wt}z^{1-s^{wt}}, \sum_{s^{wd}\in\mathcal{S}^{wd}}\mathrm{Pr}_i^{s^{wd}}z^{s^{wd}}\right\} \\
&= \sum_{s^{wd}\in\mathcal{S}^{wd}}\mathrm{Pr}_i^{s^{wd}}\left(A_{i,l}^{wt}z^{s^{wt}s^{wd}} + U_{i,l}^{wt}z^{(1-s^{wt})s^{wd}}\right)
\end{aligned}
\tag{12}
$$

where $u_{i,l}^{wi}(z)$ and $u_i^{wd}(z)$ are the UGFs of the inherent state transition of wind turbine and the wind speed, respectively; $A_{i,l}^{wt}$ and $U_{i,l}^{wt}$ are the availability and unavailability of the wind turbine, respectively; $\mathrm{Pr}_i^{s^{wd}}$ is the probability of state s^{wd} of wind speed; $\mathcal{S}^{wd}$ is the set of wind speed states.

Thus, the UGF of the wind farm $u_{i,l}^{wf}(z)$ can be written as [26]:

$$
\begin{aligned}
u_{i,l}^{wf}(z) &= \Omega^p\left\{u_{i,1}^{wt}(z),...,u_{i,l}^{wt}(z),...,u_{i,L_i^{wt}}^{wt}(z)\right\} \\
&= \sum_{s^{wd}\in\mathcal{S}^{wd}}\mathrm{Pr}_i^{s^{wd}}\left(\sum_{l=1}^{L_i^{wt}}\prod_{l'=1}^{l}A_{i,l}^{wt}\right. \\
&\qquad \left.\prod_{l'=l+1}^{L_i^{wt}}U_{i,l}^{wt}z^{s^{wd}(l's^{wt}+(L_i^{wt}-l')(1-s^{wt}))}\right)
\end{aligned}
\tag{13}
$$

where Ω^p is the parallel operator.

After knowing the state of the wind farm, the power generation capacity of the wind farm $g_i^{wf,max}$ can be determined:

$$
g_i^{wf,max} = s^{wt}f^{wd}(v_{i,l}^{s^{wd}})
\tag{14}
$$

where $f^{wd}(\cdot)$ is the function of power generation for the wind turbine with respect to the wind speed, which can be found in [28]. The UGFs of other IPGS components, e.g., traditional fossil power plants, and gas-fired power plants, can be formulated similarly.

III. SHORT-TERM RELIABILITY MANAGEMENT FOR IPGS

After formulating the short-term reliability model of the IPGS components, we can then formulate the reliability model of the IPGS. When the system component state changes, the reliability of IPGS may be affected. For example, if some gas sources fail, the gas supply can no longer meet the gas demand. As a result, some gas loads may be curtailed to maintain the system balance, and the gas composition may also change and fail to meet the requirement of gas demand. Therefore, here we propose a reliability management operator Ω^r to evaluate the consequences of different component failures. The consequences are measured in three aspects, i.e., electricity load curtailment, gas load curtailment, and gas composition deviation. These three aspects are also the performance indicators of the IPGS, and thus it can be modeled as a multi-state and multi-performance system:

$$
\begin{aligned}
u^{IPGS}(z_h) &= \Omega^r\left\{u_{i,l}^{ptg}(z_{h'}), u_i^{wf}(z), u_{i,l}^{tpp}(z), u_{i,l}^{gpp}(z), u_{i,l}^{gs}(z)\right\} \\
&= \sum_{s\in\mathcal{S}}\sum_{i\in\mathcal{I}}\mathrm{Pr}^s\left(z_1^{g_i^{ct}} + z_2^{q_i^{ct}} + z_3^{\chi_i^{ct}}\right)
\end{aligned}
\tag{15}
$$

where $u_{i,l}^{tpp}(z)$, $u_{i,l}^{gpp}(z)$, and $u_{i,l}^{gs}(z)$ are the UGFs of traditional fossil power plants, gas-fired power plants, and gas sources, respectively; Pr^s is the probability of the IPGS in state s; $\mathcal{I}$ is the set of buses; g_i^{ct}, q_i^{ct}, and χ_i^{ct} are the electricity load curtailment, gas load curtailment, and gas composition deviation at bus i, respectively.

The reliability management operator Ω^r is defined as an optimization model, which is used to determine the optimal electricity and gas load curtailments and gas composition deviations. It can be represented by the following compact form:

$$
\boldsymbol{x}^{ct} = \underset{\boldsymbol{x}}{\arg\min}\quad \boldsymbol{\lambda}^T\boldsymbol{x}^{ct}
\tag{16}
$$

subject to:

$$
\boldsymbol{Ag} + \boldsymbol{B} = 0
\tag{17}
$$
$$
\boldsymbol{C\chi q} + \boldsymbol{Dq} + \boldsymbol{E} = 0
\tag{18}
$$
$$
\boldsymbol{Rq}^2 + \boldsymbol{Fp}^2 = 0
\tag{19}
$$
$$
\boldsymbol{Gq} + \boldsymbol{H\chi} + \boldsymbol{Ip} + \boldsymbol{Jx}^{res} + \boldsymbol{K} \leq 0
\tag{20}
$$
$$
\boldsymbol{Lg} + \boldsymbol{Mq} + \boldsymbol{N} = 0
\tag{21}
$$
$$
\boldsymbol{x(s)}^{min} \leq \boldsymbol{x} \leq \boldsymbol{x(s)}^{max}
\tag{22}
$$

where the detailed mathematical formulations of the optimization problem can be found in Appendix.B. The structure of the optimization problem in this compact form is introduced below:

1) Objective function (16) means that the load curtailments and gas composition deviations should be penalized, where $\boldsymbol{x}^{ct} = [\boldsymbol{g}^{ct}, \boldsymbol{q}^{ct}, \boldsymbol{\chi}^{ct}]^T$; $\boldsymbol{x}$ is the set of decision

variable of the problem; $\boldsymbol{\lambda}$ is the penalty coefficient for $\boldsymbol{x}^{ct}$; $\boldsymbol{A}$, $\boldsymbol{B}$, ..., $\boldsymbol{N}$ are coefficients for constraints.

2) Equation (17) represents the constraints in the electricity system, including DC power flow constraints, and nodal electricity balance constraints. $\boldsymbol{g}$ represents the decision variables in the electricity system, including the electricity generation for generators, electricity consumption of PTGs, electricity load curtailments, electricity power flow, and voltage phase angle.

3) Equation (18) is the gas composition constraint, which involves the constraints for the gas mixing process at gas buses, the gas compositions of gas demand, and the gas-fired power plant's gas consumption. $\boldsymbol{q}$ is the gas-related decision variables, including gas demand, gas load curtailment, gas supply from gas sources, gas flow, gas production of PTGs, etc., for each gas component; $\boldsymbol{\chi}$ is the nodal gas composition. It is a bilinear constraint, which should be properly handled first before it can be tractably solved.

4) Equation (19) is the Weymouth equation, which describes the relationship between the gas flow rate and gas pressure drop [29]. $\boldsymbol{p}$ is the nodal gas pressure; $\boldsymbol{R}$ is gas constant. It is also a nonlinear constraint, which can not be handled by off-the-shelf solvers directly.

5) Equation (20) is the rest of the gas system constraints, including nodal gas balance constraints, energy conservation constraints for gas demand, etc. $\boldsymbol{x}^{res}$ is the rest of the decision variables.

6) Equation (21) is the coupling constraints, including the operating constraints of PTGs and gas-fired power plants.

7) Equation (22) is the lower and upper bounds for decision variables, including the electricity generation of different power plants, gas production of gas sources, capacities of electric branch and gas pipelines, gas compositions, etc. It is worth noting that some of the bounds are subject to the system state $\boldsymbol{s}$, as determined in the last Section. For example, if a PTG subsystem fails, the upper bound of hydrogen production may be affected.

IV. Short-Term Reliability Indices

As mentioned in Section III, the short-term reliability of the IPGS is evaluated from three aspects, electricity load curtailment, gas load curtailment, and gas composition deviation. For the first two aspects, the expected electricity demand not supplied (EDNS), $EDNS(t)$, and expected gas demand not supplied (EGNS), $EGNS(t)$, can be calculated based on the UGF of the IPGS:

$$EDNS(t) = \frac{\partial u^{IPGS}(z_m)}{\partial z_1}, \ EGNS(t) = \frac{\partial u^{IPGS}(z_m)}{\partial z_2} \tag{23}$$

The third aspect is calculated based on the deviations in the gas composition. As illustrated in Fig. 2(a), the green area is the secure gas composition range, which is defined by several gas security indices. Different countries and regions adopt different gas security indices. Without loss of generality, here we adopt the most common indices, the Wobbe index,

and flame speed factor, which are also closely related to the hydrogen injections. Thus, along with other constraints, such as gross caloric value, specific gravity, and molar fraction of hydrogen, the secure gas composition range $\mathbb{G}$ can be defined as [30]:

$$\mathbb{G} = \left\{ \chi_i \middle| WI_i^{min} \leq WI_i \leq WI_i^{max}, FS_i^{min} \leq FS_i \leq FS_i^{max}, \right.$$
$$GCV_i^{min} \leq GCV_i \leq GCV_i^{max}, S_i^{min} \leq S_i \leq S_i^{max},$$
$$\left. \chi_i^{hy,min} \leq \chi_i^{hy} \leq \chi_i^{hy,max} \right\} \tag{24}$$

where WI_i and FS_i are the Wobbe index and flame speed factor at bus i, respectively, which can be calculated according to Appendix; WI_i^{max}, WI_i^{min}, FS_i^{max}, FS_i^{min}, GCV_i^{max}, GCV_i^{min}, S_i^{max}, S_i^{min}, $\chi_i^{hy,max}$, and $\chi_i^{hy,min}$ are the upper and lower bounds of Wobbe index, flame speed factor, gross caloric value, specific gravity, and molar fraction of hydrogen at bus i, respectively.

In different possible system states, the gas compositions at different gas buses may be different, taking different coordinates in Fig. 2. The orange and blue dots represent the gas composition points that violate the upper and lower bounds of security constraints, respectively.

Their deviations to the secure gas composition range are defined as:

$$\chi_i^{ct} = \min_{\hat{\boldsymbol{\chi}}_i \in \mathbb{G}} ||\boldsymbol{\chi}_i - \hat{\boldsymbol{\chi}}_i|| \tag{25}$$

where $\hat{\boldsymbol{\chi}}_i$ is the candidate gas composition within the secure gas composition range.

With this idea, we can obtain the gas composition deviations in different system states, and corresponding Wobbe indices and flame speed factors. As shown in Fig. 2(b), as the state transfers over time, some may still be within the upper and lower bounds, and some may not. These gas composition points can also be projected as the reliability indices, as shown in Fig. 2. (c). We propose a pair of reliability indices, as shown in Fig. 2(c). The orange area represents the upper expected Wobbe index violation (EWIV) ($EWIV^u$), and the blue area represents the lower EWIV ($EWIV^d$). At a specific time point, if more sample points (each of them represents a system state) violate the upper bound with a higher degree, the reliability index $EWIV^u$ will also be higher. To calculate EWIV, the Wobbe index violation operator $\Omega^{WI,u}$ and $\Omega^{WI,d}$ are proposed to calculate the UGF of Wobbe index violations $u^{WI}(z)$:

$$u^{WI,u}(z) = \Omega^{WI,u}\{u^{IPGS}(z_3)\}$$
$$= \sum_{s \in \mathcal{S}} \sum_{i \in \mathcal{I}} \Pr^s z^{\delta(f^{WI}(\chi_i) - WI^{max})} \tag{26}$$

$$u^{WI,d}(z) = \Omega^{WI,d}\{u^{IPGS}(z_3)\}$$
$$= \sum_{s \in \mathcal{S}} \sum_{i \in \mathcal{I}} \Pr^s z^{\delta(WI^{min} - f^{WI}(\chi_i))} \tag{27}$$

where $f^{WI}(\cdot)$ is the function of the Wobbe index, as shown in the Appendix; $\delta(x)$ is a function defined as: $\delta(x) = x$ if $x > 0$; $\delta(x) = 0$ if $x \leq 0$.

This article has been accepted for publication in IEEE Transactions on Industry Applications. This is the author's version which has not been fully edited and content may change prior to final publication. Citation information: DOI 10.1109/TIA.2023.3286821
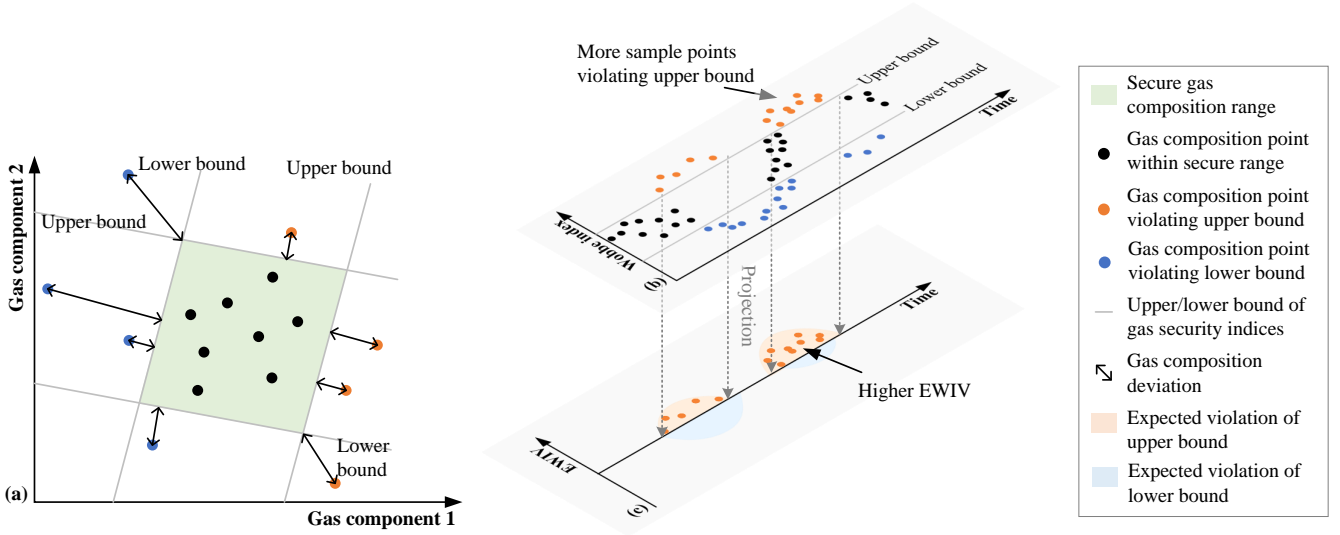
6

Fig. 2. Reliability indices for gas composition deviations: (a) secure gas composition range; (b) Wobbe index and its violations; (c) EWIV.

Then, the EWIV can be calculated as:

$$EWID^u(t) = \frac{\partial u^{WI,u}(z)}{\partial z}, \ EWID^d(t) = \frac{\partial u^{WI,d}(z)}{\partial z} \tag{28}$$

Other reliability indices, e.g., expected flame speed violation (EFSV), can be defined and calculated similarly.

V. SHORT-TERM RELIABILITY EVALUATION METHOD

A. Solution method for reliability management problem

The reliability management problem as described in Section III is a nonconvex optimization problem. The nonconvexities exist in the bilinear term in the gas mixing equations (18) and the Weymouth equation (19).

1) State-based sequential approximation of Weymouth equation: Before the injection of alternative gas, the gas composition in the gas network can be regarded as a constant, and therefore R_{ij} is also a constant. The alternative gas consists of hydrogen mostly, and sometimes with a little methane. Their gas constants are usually lower than natural gas. Therefore, we can assert that the gas constant will decrease monotonously with the increase in alternative gas injections. Because the alternative gas relies on the wind power, we can arrange the system state in an ascendant order based on the wind power $\{s_1, ..., s_h, ..., s_H\}$, where $\sum_{i \in \mathcal{I}} v_i^{s_h} \geq \sum_{i \in \mathcal{I}} v_i^{s_{h-1}}$. During the reliability evaluation, we solve the reliability management problem in scenario s_1 first, and then gradually to s_H. In each state s_h, the gas constant in the Weymouth equation is calculated based on the gas composition obtained in state s_{h-1} according to (64) in the Appendix. By this means, we can get a more accurate approximation of the gas constant without increasing the computation burden.

2) State-based McCormick envelope for gas mixing equations: The bilinear terms in the gas mixing equation (18) can be eliminated by the McCormick envelope method:

$$Dq + E + C(\chi^{min}q + \chi q^{min} - \chi^{min}q^{min}) \leq 0 \tag{29}$$
$$Dq + E + C(\chi^{max}q + \chi q^{max} - \chi^{max}q^{max}) \leq 0 \tag{30}$$

$$Dq + E + C(\chi^{max}q^{in} + \chi q^{min} - \chi^{max}q^{min}) \geq 0 \tag{31}$$
$$Dq + E + C(\chi q^{max} + \chi^{min}q - \chi^{min}q^{max}) \geq 0 \tag{32}$$

where χ^{min} and χ^{max} are the lower and upper bounds of nodal gas composition, respectively; q^{min} and q^{max} are the lower and upper bounds of q, respectively.

Though by using the McCormick envelope, the gas mixing equation is now convex, it also brings inexactness to the solution. The tightness of (29)-(32) depends on the domain knowledge of the upper and lower bounds of the approximated variables. Therefore, here we adopt a state-based bounds determination method. Similarly, we arrange the system into an ascendant order according to the wind power $\{s_1, ..., s_h, ..., s_H\}$. With more wind power, more hydrogen could be injected. Therefore, the upper and lower bounds for gas compositions are selected as ($r = 5$ is the hydrogen):

$$\chi_{i,r}^{min} = \min\{\frac{\chi_{i,l,r}^s}{1 + \chi_i^{hy,max}}, i \in \mathcal{I}, l \in \mathcal{L}_i^s\}, r = 1,2,3,4,6,7 \tag{33}$$

$$\chi_{i,r}^{max} = \max\{\chi_{i,l,r}^s, i \in \mathcal{I}, l \in \mathcal{L}_i^s\}, r = 1,2,3,4,6,7 \tag{34}$$

$$\chi_{i,r}^{min} = \chi_i^{hy,min} = 0, r = 5 \tag{35}$$

$$\chi_{i,r}^{max} = \chi_i^{hy,max} = \frac{\sum_{i \in \mathcal{I}} g_i^{ptg,s_1} \eta_{i,l}^{el}}{GCV^{hy} q_i^{in,min}}, r = 5 \tag{36}$$

$$q_i^{in,min} = q_i^{in,*}, q_i^{in,max} = q_i^{in,**} \tag{37}$$

where $q_i^{in,*}$ is the solution of q_i^{in} in the original natural gas system (without blending alternative gas); $q_i^{in,**}$ is the solution of q_i^{in} in the natural gas system where the molar fraction of hydrogen is fixed at $\chi_i^{hy,max}$ across the network. In these two scenarios, the gas compositions are both constants. The specific forms of these variables can be found in the Appendix. Therefore, the solution can be obtained by solving the traditional optimal energy flow problem [15].
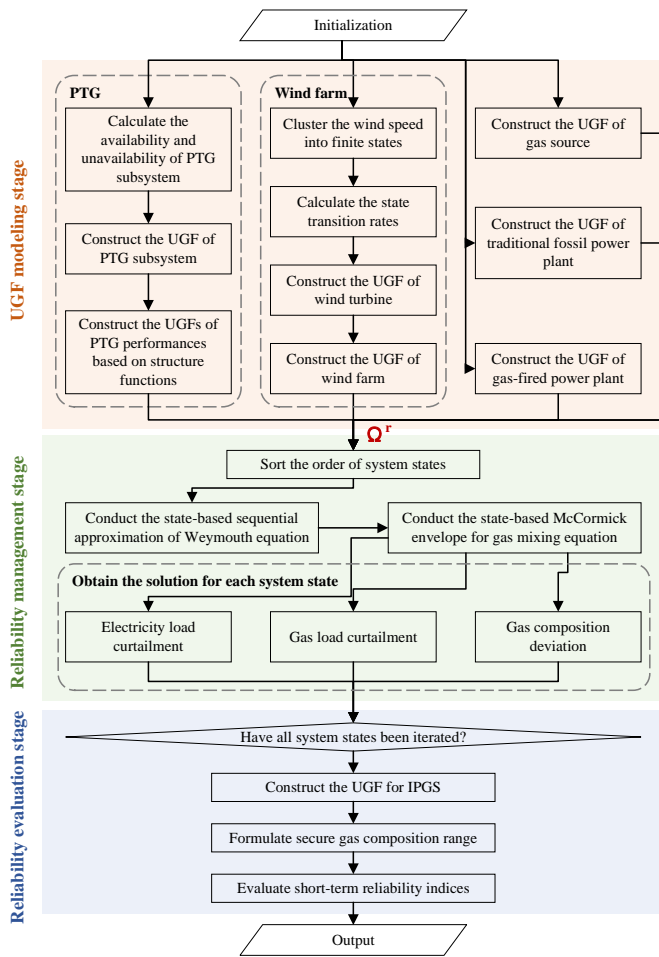
Fig. 3. Flow chart for the short-term reliability evaluation procedure.

B. Short-term reliability evaluation procedures

The short-term reliability evaluation procedure is shown in Fig.3, which is also elaborated as follows:

Step 1: Initialize the system parameters (e.g., the capacities, efficiency, failure and repair rates of generators, etc.), demand profiles (electricity load profile g_i^d and gas load profile $q_i^{d,ng}$), historical data of wind speed v_i, physical properties of gas components (e.g., gross caloric value GCV_r; gas constant R_r, etc.), and gas security parameters (e.g, lower and upper bounds of Wobbe index WI_i^{min} and WI_i^{max}, etc.) [31].

Step 2: According to Section II.A, calculate the availability and unavailability of PTG subsystems based on their failure and repair rates. Construct the UGFs of PTG subsystems. Then, obtain the UGF of the PTG based on structure functions.

Step 3: Cluster the wind speed into finite states, calculate the state transition rates, and formulate the multi-state Markov model [32]. According to Section II.B, obtain the UGFs of wind turbines, and then construct the UGFs of wind farms based on the parallel UGF operator.

Step 4: Construct the UGFs of gas sources, traditional fossil power plants, and gas-fired power plants similarly.

Step 5: Sort the order of system states according to Section V.A. For each system state, implement the state-based sequential approximation of the Weymouth equation and the state-based McCormick envelope for the gas mixing equations

according to Section V.A. Solve the reliability management problem.

Step 6: Obtain the solution of electricity/gas load curtailment and gas composition deviation. If all system states are iterated, construct the UGF of the IPGS system using the reliability management operator according to Section III.

Step 7: Formulate the secure gas composition range, and obtain the reliability indices according to Section IV.

VI. CASE STUDIES

An IPGS test case is used to validate the proposed reliability management scheme and operational reliability evaluation techniques. As shown in Fig. 4, it consists of an IEEE 24 bus Reliability Test System [33] and Belgium gas transmission system [34]. Following modifications are made: 1) the power and gas systems are topologically connected according to Fig. 4; 2) the generator # 1, 2, 5, 6, 9-11, and 16-20 are replaced with gas-fired power plants of same capacities; 3) the hydrogen production capacities of PTGs are set to 3 Mm^3/day; 4) the gas compositions natural gas, biogas, and adjustive gas are set according to the gas system in Australia [14]; 5) the 400 MW generator at electricity buses #18 is replaced by a wind farm of the same capacity. 6) The gas network has been divided into three routes according to Fig. 4. The wind data is acquired from [35]. The reliability assessment is performed on a laptop with AMD Ryzen 7 6800H CPU @3.20GHz and 32 GB RAM.

A. Validation of proposed reliability management scheme in representative system states

First, five state-of-the-art methods are compared to validate the computation efficiency of the proposed method. The description and the reason for choosing these solution methods are illustrated in Table. III. The computation time and mean error in the normal state are also presented in this table.

As we can see, the proposed method has the best performance. Compared with method B, the mean error of method A is 0.67%, which is very satisfying in the reliability evaluation. In return, the computation time is saved significantly by 96.35 %. The computation time of method C is close to method A, but the error is much higher. Method D has a better accuracy than method A, but the computation time is also significantly higher, which will cause a heavy computation burden to reliability evaluation where the optimization problem needs to be solved for numerous times. Method E also has an inferior computation efficiency and error than our method.

Then, to validate the credibility of the reliability management scheme and show the impacts of different system states on the operating conditions, six representative system states with different wind power states and component failure states are set. S1 is the normal operating state, and the wind generation is set to 400 MW. In S2, the gas source #1 fails partially by 2.32 Mm^3/day; In S3, the hydrogen purifier fails (it is assumed the gas production of PTG contains 0.5% oxygen without purification). In S4, the hydrogen buffer fails. In S5, the hydrogen compressor fails. In S6, the power generation capacity of the wind farms is reduced by 100 MW.

This article has been accepted for publication in IEEE Transactions on Industry Applications. This is the author's version which has not been fully edited and content may change prior to final publication. Citation information: DOI 10.1109/TIA.2023.3286821

8

TABLE III
COMPARISONS OF DIFFERENT SOLUTION METHODS

| Method	Description	Reason for choosing this method	Computation time (s)	Mean error
A	Proposed method	/	0.118	0.00665
B	Model stays nonlinear, and is solved by IPOPT	Straightforward, easy to implement	3.23	/
C	The reference points of the nonlinear terms (e.g., gas composition) are selected based on the initial operating state [36]	Commonly used in practical	0.103	0.117
D	Sequential programming is used [15]	An advanced method to handle nonlinearities	1.47	0.00347
E	Piece-wise linearization technique is adopted [28]	A generalized method to handle nonlinearities	0.561	0.053
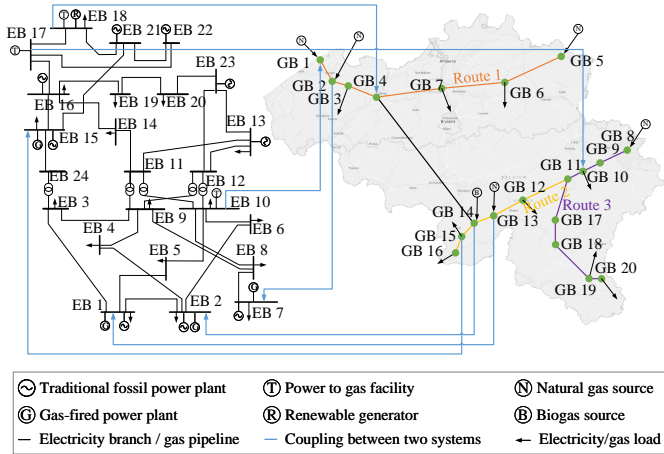
Fig. 4. IPGS test system.

The gas compositions, productions of PTGs, and gas security indices are presented in Fig. 5).

Comparing S1 and S2, we can find that gas source failure can dramatically affect the reliability of the IPGS. On the one hand, due to the gas supply shortage, although the PTGs increase their gas production, the gas loads are still curtailed for 0.0898 Mm^3/day. On the other hand, because the gas supply shortage needs to be covered, the gas production from the PTGs increase significantly by 894.29 % compared with S1, and most of it is hydrogen, as shown in Fig. 5(a). As a result, the molar fractions of hydrogen across the gas network, especially at the injection buses (e.g., #4), increase dramatically, as shown in 5(b). As shown in Fig. 5(c), due to the lower gross caloric value of hydrogen, the Wobbe index reduces significantly in most buses. At gas bus #4, the Wobbe index even exceeds the lower limit of normal state slightly by 0.86%. [1] Due to the higher flame speed of hydrogen, the flame speed factors across the gas network increase more severely. The flame speed factors at gas bus #2 and 3 violate the limit in normal conditions. At gas buses #1, 4, 7, 10-20, the gas flame speed factors even violate the limit in contingency.

From S3, we can find that the failure of the PTG purifier can lead to a slight flame speed violation in IPGS. Due to the failure of the purifier, the gas production of PTG contains oxygen. The molar fraction of oxygen is relatively small, which merely affects the operating mode of PTGs, the molar

[1]Yellow and red areas in Fig 5(c) and (d) represent the insecure gas compositions in normal states and contingent states, respectively. In other words, if the gas system is at the normal state, the security indices can not enter the yellow area; if the gas system is at contingencies, the security indices are temporally allowed to enter the yellow area. Nonetheless, in any condition, they are not allowed to enter the red area.

fraction of hydrogen, or the Wobbe index. Instead, it has more influence on the flame speed factor. Compared with S1, the flame speed factor at gas bus #4 in S3 increases by 1.92 %, which violates the limit in the normal condition slightly.

From S4 and S5, we find that the failure of the PTG buffer or compressor has little impact on the IPGS reliability. In S4, although the gas supply capability of PTG is slightly affected, the gas load will not be curtailed if other gas sources operate normally. Besides, it has little influence on the gas security indices. In S5, the PTG is no longer able to produce hydrogen. Thus, it shifts the operating mode to produce more methane. However, producing methane is less cost-efficient, and therefore the gas production of PTG is relatively low. Because the physical properties (Wobbe index, gross caloric value, etc.) of methane are closer to original natural gas than hydrogen, the Wobbe indices and flame speed factors at critical gas buses (e.g.#4, 7, 14-16) become more steady.

From S6, we can see that wind power can also affect IPGS reliability and gas security. Although wind generation is only reduced by 25%, the gas production of PTGs is almost reduced to zero. This is because the rest of the wind power tends to be used to supply electricity base load first. As a result, the hydrogen proportion is almost zero, and the Wobbe index and flame speed factor are similar to those in S1.

B. Operational Reliability Indices

Taking account of all possible system states, we can evaluate the operational reliability of the IPGS. The operational reliabilities of the IPGS are presented in Fig. 6. We can find that from the spatial dimension, different buses present different reliability patterns. For example, in the electricity system, as shown in Fig. 6(a), the electricity bus # 18 has the highest EDNS. This is because the wind farm is located at #18, which is fluctuated and causes load curtailment. The adjacent electricity buses, such as #14, #16, and #19, also have inferior reliabilities. For the gas system, as shown in Fig. 6(b), gas buses #3, #7, and #16 have the highest EGNSs, which takes about 95.49% of the total system EGNS. This is because gas bus #16 is at the end of a pipeline route, which is prone to suffer load curtailment due to the lower gas pressure. Interestingly, EWIV and EFSV present different patterns from EGNS. As shown in Fig. 6(c) and (d), gas bus #1, #4, and #10, have the highest EWIV and EFSV. This is because these three buses are the alternative gas injection points. Thus, the gas mixtures at these buses are more likely to violate the Wobbe index and flame speed factor limits.

From the temporal dimension, the reliability indices grow with time generally. This is because the system components

This article has been accepted for publication in IEEE Transactions on Industry Applications. This is the author's version which has not been fully edited and content may change prior to final publication. Citation information: DOI 10.1109/TIA.2023.3286821

9

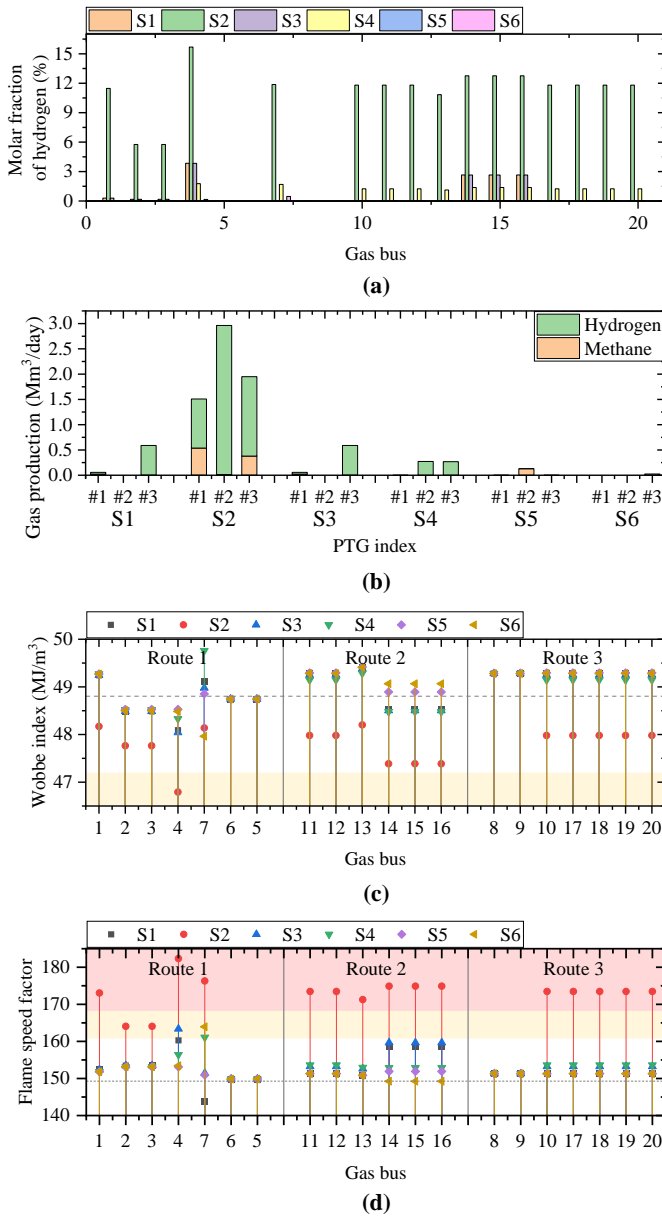

(a)

(b)

(c)

(d)

Fig. 5. Operating conditions of the IPGS in representative scenarios: (a) gas productions of PTGs; (b) molar fraction of hydrogen; (c) Wobbe index; (d)flame speed factor.

(a)

(b)

(c)

(d)

Fig. 6. Short-term reliability of IPGS: (a) EDNS; (b) EGNS; (c) EWID; (d) EWID.

(a)

(b)

(c)

(d)

Fig. 7. Comparison of short-term reliabilities of IPGS in S1-S3: (a) EDNS; (b) EGNS; (c) EWID; (d) EWID.

are in normal condition at the beginning. The probabilities of components being in the failure states gradually grow during the operation. However, during some time periods, such as 8:00-17:00, due to the higher wind power, the EDNS decreases temporally. On the contrary, the impacts of wind on the gas system reliability, such as EGNS, are not as significant as on the power system. Similarly, due to the higher wind power and hydrogen injection, the EFSV and EWIV at gas bus #10 reach the highest value at 17:00-19:00.

To further identify the main influencing factor of reliability, three scenarios are set. S1 is the base scenario. In S2, the generation capacity of the wind farm is fixed at 400 MW. In S3, the state probabilities of system components do not vary with time. Instead, they are fixed to the corresponding values at $t = 12h$. The reliability indices are presented in Fig. 7.
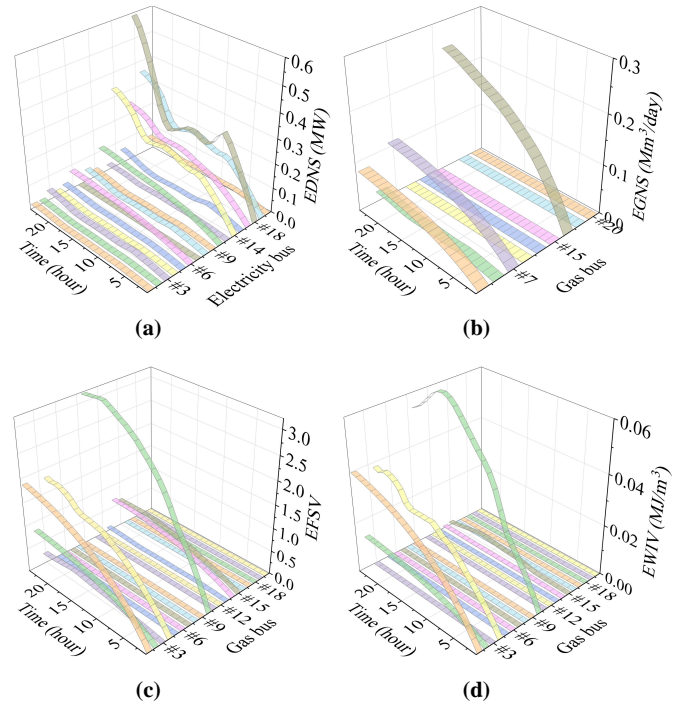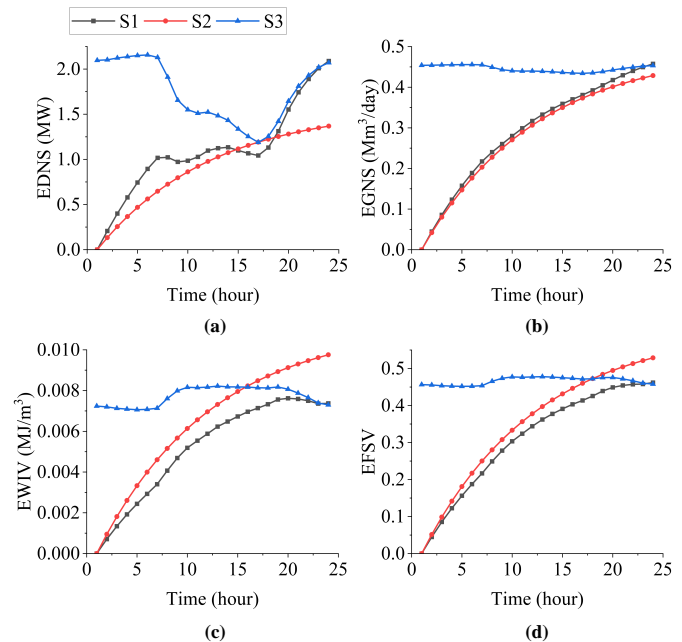
As we can find in Fig. 7(a), wind power has significant impacts on the EDNS of the power system. Compared with S2, the EDNS curve in S1 is more fluctuated. Moreover, the average EDNS in S1 is also 22.20 % higher than in S2. While in the gas system, the impact of EGNS is not so significant. Compared with S2, the EGNS in S1 is slightly higher by 4.32 %. For gas security, the EWIV and EFSV in S1 are 22.88 % and 11.63 % higher than in S2, respectively. This indicates that although the hydrogen itself will deviate the gas composition from the security range, it can still improve

the gas system reliability in general when system component failures are considered.

VII. Conclusions

This paper proposes a short-term reliability assessment method for IPGS considering alternative gas injections using the UGF method. Based on the simulation results, we can validate that the proposed reliability assessment approach can improve the computation efficiency significantly by 97.31%. We also find that though injecting the alternative gas produced by renewable generations may increase the risk of gas security violation, it is still beneficial for IPGS reliability in general. The EWIV and EFSV can be improved by 22.88% and 11.63%, respectively.

With the growing concerns for the decarbonization of energy systems, the utilization of alternative gas will attract more attention in the future. However, the risk that comes with the alternative gas can not be omitted. The proposed short-term reliability evaluation method can provide an effective tool for the system operator to manage the reliability of IPGS with alternative gas injections.

Appendix

A. Feasible region of PTG in different states

In different states, the feasible region for PTG operation is different, as shown in (8). The operating condition vector of PTG $q_{i,l}^{ptg}$ consists of:

$$q_{i,l}^{ptg} = \left[q_{i,l}^{me} + q_{i,l}^{me,ds} - q_{i,l}^{me,ch}, q_{i,l}^{hy} + q_{i,l}^{hy,ds} - q_{i,l}^{hy,ch}, q_{i,l}^{ox} \right] \tag{38}$$

where $q_{i,l}^{me}$, $q_{i,l}^{hy}$, and $q_{i,l}^{ox}$ represent the gas productions of methane, hydrogen, and oxygen, respectively; $q_{i,l}^{hy,ch}$, $q_{i,l}^{me,ch}$, $q_{i,l}^{hy,ds}$, and $q_{i,l}^{me,ds}$ are the charging and discharging gas flow rates of hydrogen and methane, respectively.

The feasible region $\mathcal{Q}_{i,l}(s)$ consists of following constraints:

1) Energy conversion constraints:

$$g_{i,l}^{ptg}\eta_{i,l}^{el} = (1 + s_1 M)GCV^{hy}(q_{i,l}^{hy} + q_{i,l}^{hy,ch} - q_{i,l}^{hy,ch})$$
$$+ GCV^{me}/\eta_{i,l}^{me}(1 + s_4 M)(q_{i,l}^{me} + q_{i,l}^{me,ch} - q_{i,l}^{me,ch}) \tag{39}$$
$$0 \le g_{i,l}^{ptg} \le (1 - s_1)g_{i,l}^{ptg,max} \tag{40}$$

where $g_{i,l}^{ptg}$ is the power consumption of the PTG; $\eta_{i,l}^{el}$ and $\eta_{i,l}^{me}$ are the efficiencies of electrolyzer and methanation reactor, respectively; GCV^{hy} and GCV^{me} are the gross caloric values of hydrogen and methane, respectively; M is a very large number.

2) Gas storage constraints:

$$Q_{i,l,k}^{hy} = Q_{i,l,k-1}^{hy} + q_{i,l,k}^{hy,ch} - q_{i,l,k}^{hy,ds} \tag{41}$$
$$Q_{i,l,k}^{me} = Q_{i,l,k-1}^{me} + q_{i,l,k}^{me,ch} - q_{i,l,k}^{me,ds} \tag{42}$$
$$0 \le \left[Q_{i,l}^{hy}, Q_{i,l}^{me} \right] \le \left[Q_{i,l}^{hy,max}, Q_{i,l}^{me,max} \right] \tag{43}$$
$$0 \le \left[q_{i,l,k}^{hy,ch}, q_{i,l,k}^{hy,ds} \right] \le s_3 \left[q_{i,l,k}^{hy,ch,max}, q_{i,l,k}^{hy,ds,max} \right] \tag{44}$$
$$0 \le \left[q_{i,l,k}^{me,ch}, q_{i,l,k}^{me,ds} \right] \le s_6 \left[q_{i,l,k}^{me,ch,max}, q_{i,l,k}^{me,ds,max} \right] \tag{45}$$

where $Q_{i,l,k}^{hy}$ and $Q_{i,l,k}^{me}$ are the storages of hydrongen and methane at time k, respectively; α^{hy} and α^{me} are the proportions of oxygen in the hydrogen and mathane productions, respectively; $g_{i,l}^{ptg,max}$ is the maximum electricity consumption of the PTG; $Q_{i,l}^{hy,max}$ and $Q_{i,l}^{me,max}$ are the storage capacities of hydrogne and mathane buffers, respectively; $q_{i,l}^{hy,ch,max}$, $q_{i,l}^{me,ch,max}$, $q_{i,l}^{hy,ds,max}$, and $q_{i,l}^{me,ds,max}$ are the maximum charging and discharging gas flow rates of hydrogen and methane, respectively.

3) Impurity constraints:

$$q_{i,l}^{ox} = s_2\alpha^{hy}(q_{i,l}^{hy} + q_{i,l}^{hy,ch}) + s_5\alpha^{me}(q_{i,l}^{me} + q_{i,l}^{me,ch}) \tag{46}$$
$$q_{i,l}^{hy}, q_{i,l}^{me} \ge 0 \tag{47}$$

B. Mathematical formulation for reliability management problem

The detailed mathematical model of the reliability management problem in (16) - (22) is elaborated as follows:

1) Objective function: The objective function of the reliability management operator is to minimize the equivalent total cost, as shown in (48). It includes electricity and gas load curtailment, and gas composition deviation costs:

$$\min_{\boldsymbol{x}} C = \sum_{i \in \mathcal{I}} \lambda^e g_i^{ct} + \lambda^g q_i^{ct} + \lambda^\chi \chi_i^{ct} \tag{48}$$
$$\boldsymbol{x} = \{g_i^{ct}, q_i^{ct}, \chi_i^{ct}, g_{i,l}^{tpp}, g_{i,l}^{gpp}, g_i^{wf}, g_{i,l}^{ptg}, g_{ij},$$
$$\theta_i, q_{i,l,r}^{gpp}, q_{i,r}^d, q_{i,l}^s, q_{ij,r}, p_i, q_{i,l,r}^{ptg}, \chi_{i,r}\} \tag{49}$$

where C is the total cost; λ^e, λ^g, and λ^χ are the penalty coefficients for electricity and gas load curtailments, and gas composition deviation, respectively; The decision variables are shown in (49), including: 1) electricity load curtailment g_i^{ct}, gas load curtailment q_i^{ct}, and gas composition deviation χ_i^{ct}; 2) electricity generation of traditional fossil power plant $g_{i,l}^{tpp}$, gas-fired power plant $g_{i,l}^{gpp}$, and wind farm g_i^{wf}; 3) electricity consumption of power-to-gas (PTG) $g_{i,l}^{ptg}$; 4) electricity flow on the electric branch g_{ij}; 5) voltage phase angle θ_i; 6) consumption of gas component r by gas-fired power plant $q_{i,l,r}^{gpp}$; 7) consumption of gas composition r by gas demand $q_{i,r}^d$; 8) gas supply from gas source $q_{i,l}^s$; 9) gas flow in pipeline for gas component r $q_{ij,r}$; 10) gas pressure p_i; 11) gas production of PTG $q_{i,l,r}^{ptg}$; 12) nodal gas composition $\chi_{i,r}$.

There are three parts of penalties in (48) for electricity load curtailment, gas load curtailment, and gas composition deviation, respectively. The penalty for electricity load curtailment essentially stands for the interruption cost of an unserved electricity load. For example, if the electricity supply for a production line is interrupted, it will cause a shutdown of the production line, and cause economic losses. In previous studies, this kind of interruption cost is usually measured by customer damage function (CDF) [37]. CDF is associated with the customer sector (residential, industrial, etc.), duration of the interruption, the power of unserved load, etc. In our case, we assume the customer sector and the interruption duration are constant. Thus, the value of CDF can be simplified as the penalty factor λ^e.

The penalty for gas load curtailment is similar. Different from the electricity CDF, there lacks of research on gas CDF. Without loss of generality, here we can calculate the gas CDF based on the electricity CDF based on the energy equivalence principle, as introduced in [38], [39]. After we obtained the gas CDF, it can be set as the penalty coefficient λ^g. The penalty coefficient for gas composition deviation stands for the economic loss when a customer is served with unqualified gas. For example, if the customer is served with gas with a lower gross caloric value, then it can not produce the same amount of heat energy as it is expected to. Then, the performance of the gas appliance will be affected. However, because the study on hydrogen blending is still at an early stage, there lacks study that can quantify the economic loss by unqualified gas. Thus, here we set the penalty coeeficient λ^χ to a number that is a bit smaller than λ^e and λ^g. By this means, the optimization problem will minimize the electricity/gas load curtailment first, and then minimize the gas composition deviation.

In addition, in our reliability management problem, we assume the system's ramping capacity can always satisfy the needs due to the participation of gas-fired generating power plants. Because we focus on load curtailment rather than economic cost, the allocation of ramping demands on generators will not affect the final results. Therefore, the optimization problem is formulated in a time-independent manner, and the computation efficiency can be significantly improved.

2) Power system constraints: The power system is formulated using the DC power flow model as follows. Eq. (50) is the nodal power balance constraint; Eq. (51) is the power flow equation; Eq. (52)-(55) are the capacities for power branches, traditional fossil power plants, gas-fired power plants, and wind farms, respectively; Eq. (56) is the energy conversion efficiency of gas-fired power plants [40].

$$\sum_{l \in \mathcal{L}_i^{tpp}} g_{i,l}^{tpp} + \sum_{l \in \mathcal{L}_i^{gpp}} g_{i,l}^{gpp} + g_i^{wf} - \sum_{l \in \mathcal{L}_i^{ptg}} g_{i,l}^{ptg}$$
$$- g_i^d - \sum_{j \in \mathcal{J}_i} g_{ij} + g_i^{ct} = 0 \quad (50)$$

$$g_{ij} = (\theta_i - \theta_j)/X_{ij} \quad (51)$$

$$|g_{ij}| \leq g_{ij}^{max} \quad (52)$$

$$g_{i,l}^{tpp,min,s^{tpp}} \leq g_{i,l}^{tpp} \leq g_{i,l}^{tpp,max,s^{tpp}} \quad (53)$$

$$g_{i,l}^{gpp,min,s^{gpp}} \leq g_{i,l}^{gpp} \leq g_{i,l}^{gpp,max,s^{gpp}} \quad (54)$$

$$g_i^{wf,min,s^{wf}} \leq g_i^{wf} \leq g_i^{wf,max,s^{wf}} \quad (55)$$

$$g_{i,l}^{gpp} = \eta_{i,l}^{gpp} \sum_{r \in \mathcal{R}} q_{i,l,r}^{gpp} GCV_r, \ q_{i,l,r}^{gpp} \geq 0 \quad (56)$$

where $\mathcal{L}_i^{tpp}, \mathcal{L}_i^{gpp}$, and $\mathcal{L}_i^{ptg}$ are the sets of traditional fossil power plants, gas-fired power plants, and PTGs at bus i, respectively; $\mathcal{J}_i$ is the set of electricity branches connected to bus i; g_i^d is the electricity demand at bus i; X_{ij} is the reactance of branch ij; g_{ij}^{max} is the capacity of the electricity branch ij; $g_{i,l}^{tpp,max,s^{tpp}}$, $g_{i,l}^{tpp,min,s^{tpp}}$, $g_{i,l}^{gpp,max,s^{gpp}}$, $g_{i,l}^{gpp,min,s^{gpp}}$, $g_i^{wf,max,s^{wf}}$, and $g_i^{wf,min,s^{wf}}$ are the upper and lower bounds of traditional fossil power plant, gas-fired power plants, and wind farm in state s^{tpp}, s^{gpp}, and s^{wf}, respectively. Partic-

ularly for wind farms, it can be regarded as a controllable resource by pitch or yaw control [41]. Thus, the maximum power output is calculated based on (14), while the minimum output can be regarded as zero.

3) Gas system constraints: The gas system constraints are formulated as follows. Eq. (57) is the gas demand constraint, which enforces that the heat energy of the consumed gas components should equal the original heat value measured by the natural gas. Otherwise, it should be regarded as a gas load curtailment. Eq. (58) is the gas composition constraint for gas sources. It indicates that the composition of the gas produced by the gas source should be consistent. Eq. (59) is the Weymouth equation, which describes the relationship between the gas flow rate and the gas pressure drop [42]. Eq. (60) indicates that the sum of all the gas components should equal the total gas flow rate. Eq. (61) is the nodal gas flow balance, which is formulated for all gas compositions. Eqs. (62)-(63) describe the mixing process of different gas components [43]. Eq. (62) is the nodal gas injection from different gas components, including the flow-in gas from upper stream pipelines, the gas sources, and the PTGs. Eq. (63) calculates the nodal gas composition based on these gas injections. Eq. (64)-(66) calculate the specific gravities and compressibility factors in both buses and pipelines. Eq. (67) enforces that the gas composition of the downstream pipelines should be equal to the gas composition of the upper stream gas bus. Eq. (68)-(70) are the upper and lower bounds for gas sources, gas flows in the pipelines, and nodal gas pressures, respectively.

$$GCV^{ng} q_i^{d,ng} = \sum_{r \in \mathcal{R}} (q_{i,r}^d + q_{i,r}^{ct}) GCV_r, \ q_{i,r}^d, q_{i,r}^{ct} \geq 0 \quad (57)$$

$$q_{i,l,r}^s = \chi_{i,l,r}^s q_{i,l}^s, \ \sum_{r \in \mathcal{R}} \chi_{i,l,r}^s = 1 \quad (58)$$

$$q_{ij}^2 = \pi^2 D_{ij}^5 (F_{ij} R_{ij} L_{ij} Z_{ij} T^{gas})^{-1} \gamma_{ij} (p_i^2 - p_j^2) \quad (59)$$

$$q_{ij} = \sum_{r \in \mathcal{R}} q_{ij,r} \quad (60)$$

$$\sum_{l \in \mathcal{L}_i^s} q_{i,l,r}^s - q_{i,r}^d + \sum_{l \in \mathcal{L}_i^{ptg}} q_{i,l,r}^{ptg} - \sum_{l \in \mathcal{L}_i^{gpp}} q_{i,l,r}^{gpp}$$
$$- \sum_{j \in \mathcal{J}_i} q_{ij,r} = 0, \forall r \in \mathcal{R} \quad (61)$$

$$q_{i,r}^{in} = \sum_{j \in \mathcal{J}_i} (\gamma_{ij} - 1) q_{ij,r}/2 + \sum_{l \in \mathcal{L}_i^s} q_{i,l,r}^s + \sum_{l \in \mathcal{L}_i^{ptg}} q_{i,l,r}^{ptg} \quad (62)$$

$$\chi_{i,r} = q_{i,r}^{in}/q_i^{in}, \ q_i^{in} = \sum_{r \in \mathcal{R}} q_{i,r}^{in} \quad (63)$$

$$R_i = \sum_{r \in \mathcal{R}} R_r \chi_{i,r} \quad (64)$$

$$R_{ij} = ((1 + \gamma_{ij}) R_i + (1 - \gamma_{ij}) R_j)/2 \quad (65)$$

$$Z_{ij} = f_Z(\chi_i, \chi_j, p_i, p_j) \quad (66)$$

$$\chi_{ij} = q_{ij,r}/q_{ij} = ((1 + \gamma_{ij})\chi_i + (1 - \gamma_{ij}))/2 \quad (67)$$

$$q_{i,l}^{s,min} \leq q_{i,l}^s \leq q_{i,l}^{s,max} \quad (68)$$

$$(\gamma_{ij} - 1) q_{ij}^{max}/2 \leq q_{ij} \leq (\gamma_{ij} + 1) q_{ij}^{max}/2 \quad (69)$$

$$p_i^{min} \leq p_i \leq p_i^{max} \quad (70)$$

This article has been accepted for publication in IEEE Transactions on Industry Applications. This is the author's version which has not been fully edited and content may change prior to final publication. Citation information: DOI 10.1109/TIA.2023.3286821

12

where GCV^{ng} is the gross caloric value of purely natural gas; $q_i^{d,ng}$ is the gas demand measured by natural gas; GCV_r is the gross caloric value of gas component r; $q_{i,l,r}^s$ is the gas component r supplied by gas source l at bus i; q_{ij} is the gas flow rate between the bus i and j; $\chi_{i,l,r}^s$ is the molar fraction of the gas component r of gas source l at bus i; D_{ij}, L_{ij}, and F_{ij} are the diameter, length, and friction factor of the pipeline ij, respectively; R_{ij} and Z_{ij} is the gas constant and compressibility factor of the gas mixture in pipeline ij, respectively (note that these two are variables that depend on the gas composition in the pipeline, and therefore may be changing during the operation); T^{gas} is the temperature of gas; $\gamma_{ij} \in \{-1, 1\}$ is the gas flow direction, where $\gamma_{ij} = 1$ indicates that the gas flows from bus i to j, and $\gamma_{ij} = -1$ indicates otherwise; $q_{i,r}^{in}$ is the sum of gas component r that flows into the gas bus i, and q_i^{in} is the sum of all gas components that flows into the gas bus i; R_r is the gas constant of component r; $q_{i,l}^{s,max}$ and $q_{i,l}^{s,min}$ are the upper and lower bounds of the gas supply for gas source l at bus i, respectively; q_{ij}^{max} is the capacity of the gas pipeline ij; p_i^{max} and p_i^{min} are the upper and lower bounds for the nodal gas pressure at bus i, respectively; $f_Z(\cdot)$ is the function of compressibility factor with respect to the gas compositions and nodal gas pressures [44].

C. Gas security indices

Wobbe index and flame speed factor are used in this paper to measure the gas system security. The Wobbe index describes the interchangeability of gas. The similar Wobbe indices indicate that the two gas mixtures can produce identical heat energy for the given pressure and valve settings. Because the hydrogen has a lower heat value, the hydrogen injection will decrease the Wobbe index of the gas mixture. Therefore, we need to keep the Wobbe index within the appropriate range. It can be calculated as [45]:

$$WI_i = \sum_{r \in \mathcal{R}} GCV_{i,r}\chi_i / \sqrt{S_i} \tag{71}$$

The flame speed describes the maximum velocity of the flame travel in the gas-air mixture during combustion. The injection of hydrogen can increase the flame speed of the gas mixture, which may cause flashbacks. Therefore, the flame speed factor should be limited. Weaver flame speed is used in this paper [46]:

$$FS_i = \frac{\sum_{r \in R} \chi_{i,r} fs_r}{AF + 5\chi_i^{ni} - 18.8\chi_i^{ox} + 1} \tag{72}$$

where fs_r is the burning velocity of gas component r; AF is the air-fuel ratio; χ_i^{ni} is the molar fraction of nitrogen at bus i.

REFERENCES

[1] H. Hui, P. Siano, Y. Ding, P. Yu, Y. Song, H. Zhang, and N. Dai, "A transactive energy framework for inverter-based hvac loads in a real-time local electricity market considering distributed energy resources," *IEEE Transactions on Industrial Informatics*, vol. 18, no. 12, pp. 8409–8421, Feb. 2022.

[2] Mid and long-term planning of hydrogen industry development. [Online]. Available: http://zfxxgk.nea.gov.cn/2022-03/23/c_1310525630.htm.

[3] H. Hui, Y. Ding, K. Luan, T. Chen, Y. Song, and S. Rahman, "Coupon-based demand response for consumers facing flat-rate retail pricing," *CSEE Journal of Power and Energy Systems*, (early access). 2023.

[4] J. Klimstra, "Interchangeability of gaseous fuels—the importance of the wobbe-index," *SAE transactions*, pp. 962–972, 1986.

[5] O. Bouledroua, Z. Hafsi, M. B. Djukic, and S. Elaoud, "The synergistic effects of hydrogen embrittlement and transient gas flow conditions on integrity assessment of a precracked steel pipeline," *International Journal of Hydrogen Energy*, vol. 45, no. 35, pp. 18 010–18 020, Jul. 2020.

[6] C. J. Quarton and S. Samsatli, "Should we inject hydrogen into gas grids? practicalities and whole-system value chain optimisation," *Applied Energy*, vol. 275, p. 115172, Oct. 2020.

[7] S. Clegg and P. Mancarella, "Integrated modeling and assessment of the operational impact of power-to-gas (p2g) on electrical and gas transmission networks," *IEEE Transactions on Sustainable Energy*, vol. 6, no. 4, pp. 1234–1244, Oct. 2015.

[8] A. M. De Corato, S. Riaz, and P. Mancarella, "Assessing the flexibility of electricity-gas-hydrogen distribution systems with p2g units," in *2021 IEEE PES Innovative Smart Grid Technologies-Asia (ISGT Asia)*. IEEE, Nov. 2021, pp. 1–5.

[9] S. Zhang, S. Wang, Z. Zhang, J. Lyu, H. Cheng, M. Huang, and Q. Zhang, "Probabilistic multi-energy flow calculation of electricity–gas integrated energy systems with hydrogen injection," *IEEE Transactions on Industry Applications*, vol. 58, no. 2, pp. 2740–2750, Jul. 2021.

[10] D. Zhou, S. Yan, D. Huang, T. Shao, W. Xiao, J. Hao, C. Wang, and T. Yu, "Modeling and simulation of the hydrogen blended gas-electricity integrated energy system and influence analysis of hydrogen blending modes," *Energy*, vol. 239, p. 121629, Jan. 2022.

[11] D. Zhou, C. Wang, S. Yan, Y. Yan, Y. Guo, T. Shao, T. Li, X. Jia, and J. Hao, "Dynamic modeling and characteristic analysis of natural gas network with hydrogen injections," *International Journal of Hydrogen Energy*, vol. 47, no. 78, pp. 33 209–33 223, Sep. 2022.

[12] P. Zhao, C. Gu, Z. Hu, D. Xie, I. Hernando-Gil, and Y. Shen, "Distributionally robust hydrogen optimization with ensured security and multi-energy couplings," *IEEE Transactions on Power Systems*, vol. 36, no. 1, pp. 504–513, Jun. 2020.

[13] P. Zhao, X. Lu, Z. Cao, C. Gu, Q. Ai, H. Liu, Y. Bian, and S. Li, "Volt-var-pressure optimization of integrated energy systems with hydrogen injection," *IEEE Transactions on Power Systems*, vol. 36, no. 3, pp. 2403–2415, Oct. 2020.

[14] I. Saedi, S. Mhanna, and P. Mancarella, "Integrated electricity and gas system modelling with hydrogen injections and gas composition tracking," *Applied Energy*, vol. 303, p. 117598, Dec. 2021.

[15] S. Wang, J. Zhai, and H. Hui, "Optimal energy flow in integrated electricity and gas systems with injection of alternative gas," *IEEE Transactions on Sustainable Energy*, (early access). 2023.

[16] C. Juanwei, Y. Tao, X. Yue, C. Xiaohua, Y. Bo, and Z. Baomin, "Fast analytical method for reliability evaluation of electricity-gas integrated energy system considering dispatch strategies," *Applied Energy*, vol. 242, pp. 260–272, May. 2019.

[17] H. Hui, Y. Chen, S. Yang, H. Zhang, and T. Jiang, "Coordination control of distributed generators and load resources for frequency restoration in isolated urban microgrids," *Applied Energy*, vol. 327, p. 120116, Dec. 2022.

[18] T. Wu and J. Wang, "Reliability evaluation for integrated electricity-gas systems considering hydrogen," *IEEE Transactions on Sustainable Energy*, Dec. 2022.

[19] C. K. Wu and C. K. Law, "On the determination of laminar flame speeds from stretched flames," in *Symposium (International) on Combustion*, vol. 20, no. 1. Elsevier, 1985, pp. 1941–1949.

[20] Y. Chen, D. Qi, H. Hui, S. Yang, Y. Gu, Y. Yan, Y. Zheng, and J. Zhang, "Self-triggered coordination of distributed renewable generators for frequency restoration in islanded microgrids: A low communication and computation strategy," *Advances in Applied Energy*, vol. 10, p. 100128, Jun. 2023.

[21] S. Wang, L. Zhou, L. Zhong, X. Wang, W. Shi, F. Zou, and Y. Ma, "Steady-state optimal power flow in integrated electricity and gas transmission systems with hydrogen injections," in *2022 IEEE/IAS Industrial and Commercial Power System Asia (I&CPS Asia)*. IEEE, 2022, pp. 2025–2030.

[22] M. Bao, Y. Ding, C. Singh, and C. Shao, "A multi-state model for reliability assessment of integrated gas and power systems utilizing

This article has been accepted for publication in IEEE Transactions on Industry Applications. This is the author's version which has not been fully edited and content may change prior to final publication. Citation information: DOI 10.1109/TIA.2023.3286821

13

universal generating function techniques," *IEEE Transactions on Smart Grid*, vol. 10, no. 6, pp. 6271–6283, Feb. 2019.

[23] G. Levitin *et al.*, *The universal generating function in reliability analysis and optimization*. Springer, 2005, vol. 6.

[24] J. Su, H. Zhang, H. Liu, L. Yu, and Z. Tan, "Membership-function-based secondary frequency regulation for distributed energy resources in islanded microgrids with communication delay compensation," *IEEE Transactions on Sustainable Energy*, (early access). 2023.

[25] H. Hui, M. Bao, Y. Ding, and Y. Song, "Exploring the integrated flexible region of distributed multi-energy systems with process industry," *Applied Energy*, vol. 311, p. 118590, Apr. 2022.

[26] Y. Ding, C. Singh, L. Goel, J. Østergaard, and P. Wang, "Short-term and medium-term reliability evaluation for power systems with high penetration of wind power," *IEEE Transactions on Sustainable Energy*, vol. 5, no. 3, pp. 896–906, Apr. 2014.

[27] S. Wang, H. Hui, Y. Ding, C. Ye, and M. Zheng, "Operational reliability evaluation of urban multi-energy systems with equivalent energy storage," *IEEE Transactions on Industry Applications*, vol. 59, no. 2, pp. 2186–2201, Mar-Apr. 2022.

[28] M. Bao, Y. Ding, C. Shao, Y. Yang, and P. Wang, "Nodal reliability evaluation of interdependent gas and power systems considering cascading effects," *IEEE Transactions on Smart Grid*, vol. 11, no. 5, pp. 4090–4104, Sep. 2020.

[29] M. Bao, H. Hui, Y. Ding, X. Sun, C. Zheng, and X. Gao, "An efficient framework for exploiting operational flexibility of load energy hubs in risk management of integrated electricity-gas systems," *Applied Energy*, vol. 338, p. 120765, May. 2023.

[30] Gas Safety (Management) Regulations. [Online]. Available: https://www.legislation.gov.uk/uksi/1996/551/introduction/made.

[31] L. Yan, X. Chen, Y. Chen, and J. Wen, "A cooperative charging control strategy for electric vehicles based on multiagent deep reinforcement learning," *IEEE Transactions on Industrial Informatics*, vol. 18, no. 12, pp. 8765–8775, Dec. 2022.

[32] S. Wang, J. Zhai, H. Hui, Y. Ding, and Y. Song, "Operational reliability of integrated energy systems considering gas flow dynamics and demand-side flexibilities," *IEEE Transactions on Industrial Informatics*, (early access). 2023.

[33] C. Ordoudis, P. Pinson, J. M. Morales, and M. Zugno, "An updated version of the ieee rts 24-bus system for electricity market and power system operation studies," *Technical University of Denmark*, vol. 13, 2016.

[34] J. Munoz, N. Jimenez-Redondo, J. Perez-Ruiz, and J. Barquin, "Natural gas network modeling for power systems reliability studies," in *2003 IEEE Bologna Power Tech Conference Proceedings,*, vol. 4. IEEE, Jun. 2003, pp. 8–pp.

[35] National oceanic and atmospheric administration. [Online]. Available: https://www.noaa.gov/.

[36] C. Wang, K. Wu, H. Liu, Q. Jia, and T. Bi, "Optimal gas-power flow calculation with lightweight gas flow dynamics," *IEEE Transactions on Smart Grid*, vol. 14, no. 2, pp. 965–978, Mar. 2022.

[37] S. Wang, Y. Ding, C. Ye, C. Wan, and Y. Mo, "Reliability evaluation of integrated electricity–gas system utilizing network equivalent and integrated optimal power flow techniques," *Journal of Modern Power Systems and Clean Energy*, vol. 7, no. 6, pp. 1523–1535, Nov. 2019.

[38] A. Helseth and A. T. Holen, "Impact of energy end use and customer interruption cost on optimal allocation of switchgear in constrained distribution networks," *IEEE transactions on power delivery*, vol. 23, no. 3, pp. 1419–1425, Jul. 2008.

[39] S. Wang, C. Shao, Y. Ding, and J. Yan, "Operational reliability of multi-energy customers considering service-based self-scheduling," *Applied Energy*, vol. 254, p. 113531, Nov. 2019.

[40] S. Yang, K.-W. Lao, H. Hui, Y. Chen, and N. Dai, "Real-time harmonic contribution evaluation considering multiple dynamic customers," *CSEE Journal of Power and Energy Systems*, (early access). 2023.

[41] Exploring the fundamental concepts and control methods/techniques for wind-turbine control systems. [Online]. Available: https://www.windsystemsmag.com/wind-turbine-control-methods/.

[42] C. M. Correa-Posada and P. Sánchez-Martın, "Security-constrained optimal power and natural-gas flow," *IEEE Transactions on Power Systems*, vol. 29, no. 4, pp. 1780–1787, Jan. 2014.

[43] Resilience of gas interchangeability in hydrogen-blended integrated electricity and gas systems: A transient approach with dynamic gas composition tracking. [Online]. Available: https://github.com/ShengWang-EE/Resilience-of-Gas-Interchangeability-in-Hydrogen-Blended-Integrated-\Electricity-and-Gas-Systems-A-T.

[44] G. Soave, "Equilibrium constants from a modified redlich-kwong equation of state," *Chemical engineering science*, vol. 27, no. 6, pp. 1197–1203, 1972.

[45] I. O. for Standardization, *Natural Gas: Calculation of Calorific Values, Density, Relative Density and Wobbe Index from Composition*. International Organization for Standardization, 1995.

[46] E. R. Weaver, "Formulas and graphs for representing the interchangeability of fuel gases," *Journal of Research of the National Bureau of Standards*, vol. 46, no. 3, pp. 213–245, 1951.

Sheng Wang (Member) received both the Ph.D. and B. Eng degrees in electrical engineering from Zhejiang University in 2021 and 2016, respectively. He was with the State Grid (Suzhou) City & Energy Research Institute in 2021. He is currently a Postdoctoral Fellow with the State Key Laboratory of Internet of Things for Smart City, University of Macau. His research interests include the optimization and reliability evaluation of integrated energy systems and the low-carbon strategy for urban energy systems.

Hongxun Hui (Member) received the B.E. and Ph.D. degrees in electrical engineering from Zhejiang University, Hangzhou, China, in 2015 and 2020, respectively. From 2018 to 2019, he was a visiting scholar at the Advanced Research Institute at Virginia Tech, and the CURRENT Center in the University of Tennessee. He is currently a Research Assistant Professor with the State Key Laboratory of Internet of Things for Smart City, University of Macau, Macao SAR, China. His research interests include optimization and control of power systems, demand response, and Internet of Things technologies for smart energy.

Junyi Zhai (Member) received the B.S. and Ph.D. degrees in electrical engineering from North China Electricity Power University, Beijing, China, in 2014 and 2019, respectively. He was a visiting student at the University of Birmingham during 2018 and 2019. He was a senior research engineer at the State Grid (Suzhou) City & Energy Research Institute in 2019 and 2022. His research interests include mathematical optimization techniques and power system analysis and computing.